IET Generation, Transmission & Distribution

Special Issue: Distributed & Autonomous Dispatch and Control for Active Distribution Networks/Microgrids Potential Scheme to Realise Plug & Play of DER

Approach to setting gateway reactive power control band for distribution networks with wind power

ISSN 1751-8687
Received on 26th April 2016
Revised on 6th September 2016
Accepted on 6th September 2016
doi: 10.1049/iet-gtd.2016.0620
www.ietdl.org

Xu Chen, Yingqi Yi, Yongjun Zhang ✉, Qinhao Li, Jianquan Zhu, Zexiang Cai

School of Electric Power Engineering, South China University of Technology, No. 381, Wushan Road, Guangzhou, People's Republic of China
✉ *E-mail: zhangjun@scut.edu.cn*

Abstract: The integration of distributed wind farm leads to additional fluctuation of power flow in a high-voltage distribution network, which has become a major concern in automatic voltage control. This study proposes a slack optimal control method to determine the tolerance band of gateway reactive power (GRP) which takes into account voltage constraints, energy loss and excessive operations of control devices. Analysis of network characteristics shows that the GRP control band should be set according to both load levels and the outputs of distributed wind farm. Based on the analysis, slack optimal active loss difference strategy is proposed to set the slack optimal band of GRP. A slack optimal band matrix is defined and a partitioning intersection strategy is proposed to implement the differential setting of the slack optimal control band parameters of GRP. Simulation studies are conducted on a practical distribution network in China and the results show that the proposed method performs well in energy saving, control device regulating, voltage profile keeping, and reactive power balancing in a simple and practical way.

1 Introduction

Recent years have seen fast development of wind power generation [1]. In addition to large centralised wind farms which are directly connected to transmission networks, there are more than 1000 distributed wind farms whose capacity ranges between 10 and 99 MW scattered in 110 kV high-voltage distribution networks in China. The distributed wind farms are usually chained with substations by lines from remote areas where the natural condition of wind is good [2, 3], as shown in Fig. 1. Integration of the distributed wind farms in radial high-voltage distribution networks can significantly affect the power flows, which in turn leads to the increase in voltage violation rate [4–6], system loss [7, 8] and frequency of control devices regulation [9, 10].

Automatic voltage control (AVC) system is developed to solve these voltage and reactive power problems in power grids. How to coordinate the on-load-tap-changer (OLTC) and shunt capacitors in a substation [11, 12] to reduce the negative impact of introduction of distributed wind farms has been a challenge to the existing AVC system. The AVC approach has been discussed widely [13–28], which can be classified into two categories.

The first approach is 'centralised control method' [13–17] which is a straightforward solution that maximises the control performance. In [14], a robust optimisation model was proposed to coordinate the discrete and continuous reactive power compensators and find a robust optimal solution in consideration of large centralised wind farms integration. In [15, 16], the doubly-fed induction generators in the wind farm were treated as a continuous reactive power source in the reactive power optimisation (RPO) in a distribution network, the objective of which was to minimise the power loss of the system. Although these approaches can obtain the global optimal solution in theory, especially for small systems, they require reliable communication link among sensors, voltage control devices and the distribution network control centre, which means a large investment as well as special attention are required for reliability against system faults [18]. Ahmed [19] indicated the optimisation problem is always formulated as a single step optimisation problem which cannot be robust to various uncertainties or change in system properties. Furthermore, for a large power system with time-varying operation condition, modelling of topology of the power system may become so complicated that the computational burden of control centre increases dramatically [20]. Therefore, it is difficult to apply the optimisation based centralised control method in practice.

The second approach is 'local control method' [21–28] which performs real-time control based on local measurements. An optimal parameter setting and a dead band control for OLTC were shown in [22, 23]. In [24], a control coordination technique based on the concepts of control zone, line drop compensation, dead band, as well as the choice of controllers' parameters was proposed to minimise the interaction with other active devices. Afandi *et al.* [25] proposed an integrated volt/VAr control (IVVC) to improve the overall voltage profile and reduce the total number of tap operations in middle-voltage distribution networks. Reference [27] proposed a nine-area control algorithm which is widely adopted as the local control method of the substation in China considering its simplicity and practicality [28]. These approaches, which focus on the coordinated control of OLTC and shunt capacitor, are in general reliable due to their independency and simplicity of control system configuration. However, the drawback of these approaches is that the power loss cannot be reduced effectively, and their control effect highly depends on the control parameters which are usually fixed and cannot change with the variation of operation status.

Overall, AVC system can hardly achieve its objectives such as power loss saving, voltage keeping, and regulation time minimising simultaneously when the load demand of system and the output of wind power varied violently and asynchronously. Although there are a lot of research works about voltage and reactive power control in distribution system with wind farms, these researches tend to focus on the coordination of OLTC in substation and reactive power control of wind farm, and capacitor switching on the feeders. There is few references to discuss the influence of intermittent wind power on the volt/VAr control in substation, or to investigate the AVC strategies to adapt the fluctuant wind power integrated into the high-voltage distribution network.

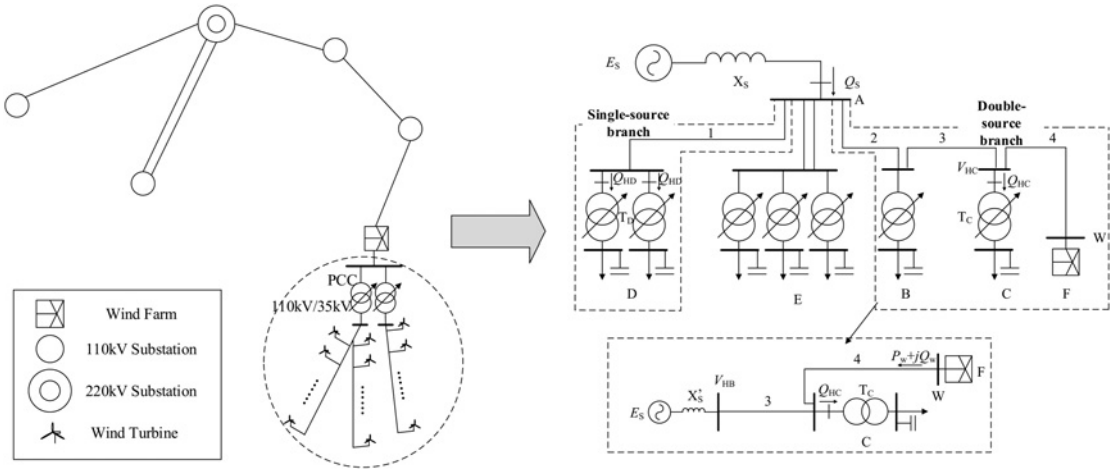

Fig. 1 *Typical high-voltage distribution network with a wind farm integration*

This paper therefore aims at the volt/VAr control of high-voltage distribution network with distributed wind farms integration and an improved local control method, slack optimal control, is proposed. The contributions of this paper include:

(i) Correlation characteristics between the reactive power injected from the upstream network to the substation primary bus (i.e. gateway reactive power (GRP)), and the active loss of branches in radial high-voltage distribution networks have been investigated with and without wind farms, respectively.
(ii) A strategy to set the slack optimal control band of GRP in consideration of the uncertainty of load level and distributed wind farm output has been proposed.
(iii) A slack optimal method which is based on the nine-area control algorithm [27, 28] has been proposed to coordinate the controls of OLTC and shunt capacitors in substation, and the control parameters of the proposed method are adjusted for the power flow fluctuation caused by wind farms.

The paper is organised as follows. Section 2 proposes a slack optimal method. In Section 3, the setting strategies of the optimal control band of GRP selection for single-source and double-source branches are presented. In Section 4, the setting process of slack optimal band of GRP for typical situation is demonstrated, and simulation studies are carried out to demonstrate the effectiveness of the proposed method, in comparison with the methods proposed in recent literatures. Finally, conclusions are drawn in Section 5.

2 Slack optimal control formulation

Three objectives are usually included for AVC, such as minimising power loss, avoiding voltage violation and reducing the operation times of discrete control devices, but it is not easy to fulfil them simultaneously [29]. The costs of adjusting the control devices are added to the power losses to construct an objective function which can balance these objectives [30], since the power loss objective is sacrificed to reduce the operation times.

For the local control method, the branch power loss can be thought as the minimum one when the corresponding GRP is controlled near 0, since the reactive power flow is nearly minimised. Moreover, an experiential slack control band of GRP is adopted for AVC to reduce the operation times at the cost of power loss rising. However, how to determine the parameters of control band of GRP to balance these objectives is a key to the local control method, especially under time-varying loads and fluctuant wind power. As an improved local control method, the proposed slack optimal control is therefore to settle this key problem.

2.1 Slack optimal control objective

The objective of slack optimal control is to find a 'slack' optimal solution which may be close to the minimum power loss meanwhile reduce the operation times, and its objective function can be expressed as

$$F = P_{\mathrm{LOSS},i} \in [P_{\min,i},\ P_{\min,i} + \Delta P] \tag{1}$$

where $P_{\mathrm{LOSS},i}$ represents the system loss in scenario i; $P_{\min,i}$ represents the minimum system loss can be reached by RPO in scenario i; ΔP is called *slack optimal active loss difference*, which can be expressed as

$$\Delta P = \alpha \cdot P_{\min.\max} \tag{2}$$

where $P_{\min.\max}$ represents the maximum value of $P_{\min,i}$ in all scenarios; α is defined as *slack optimisation cost* which represents the percentage of the maximum difference between $P_{\min.\max}$ and the power loss at other operating points in a GRP band. Obviously, the larger ΔP, the less power loss saving and the less operation times can be expected.

2.2 Slack optimal control constraints

High-voltage distribution network generally operates in radial connection modes. Since the wind farms are usually chained with terminal substations by lines from remote areas, as shown in Fig. 1, the line-transformer units on the chain from a pilot bus to a wind farm are named double-source branches (e.g. the branches including Substations C and B along with Lines 2–4), and the other branches are called single-source branches (e.g. the branch including Substation D along with Line 1). F is the wind farm, W is the access point of the wind farm and A is the pilot bus which represents the access point to upstream grid. In the high-voltage distribution network with wind farms integration, the voltage constraints are expressed as

$$U^{\min} \le U_{j,i} \le U^{\max}, \quad \forall j \in B_N \backslash \Omega_{\mathrm{B}} \tag{3}$$

$$U^{\min} + \varepsilon \le U_{j,i} \le U^{\max} - \varepsilon, \quad \forall j \in \Omega_{\mathrm{B}} \tag{4}$$

where B_N is the set of buses; Ω_{B} is set of the primary buses of substation in double-source branch; $j \in B_N \backslash \Omega_{\mathrm{B}}$ denotes $j \in B_N$, but $j \notin \Omega_{\mathrm{B}}$; $U^{\min}$ is minimum allowed voltage; $U^{\max}$ is maximum allow voltage; ε is defined as voltage safety margin which is set in consideration of uncertainty of the distributed wind farm output; and $U_{j,i}$ is the voltage at bus j in scenario i.

2.3 Slack optimal control algorithm

The slack optimal control algorithm is based on the nine-area control algorithm, which has been widely adopted as the local control strategy for a commercial AVC system in the substation to make a balance between the local reactive power and the voltage quality. Taking the substation secondary voltage V_L and GRP Q_H as the variables to form a two-dimensional plane, nine areas are divided by V_{Lmax}, V_{Lmin}, Q_{Hmax} and Q_{Hmin}. Here, V_{Lmax} and V_{Lmin} represent the maximum and minimum allowable secondary voltages, respectively, and Q_{Hmax} and Q_{Hmin} represent the maximum and minimum allowable GRPs, respectively.

As shown in Fig. 3, Area 5 is considered as the only qualified area. Its voltage is between the pre-set upper and lower limits, and its reactive power is controlled within a pre-set band. If the operation status falls in other areas, it needs further adjustments, such as capacitor switching and transformer tap changing, to enter into Area 5. As shown in Fig. 2, C+ and C− denote switching on and off capacitor banks, respectively, while T+ and T− mean turning up and down OLTCs, respectively.

2.4 Slack optimal control parameters

The nine-area control algorithm is simple and practical, but the control effect highly depends on the control parameters which are usually set empirically. Among these parameters, the control band of GRP (i.e. Q_{Hmin} and Q_{Hmax}) is the key factor which indicates the regional reactive power balance condition [31]. The simulation results presented in [32] have indicated that the nine-area control algorithm cannot guarantee the minimum real power loss when keeping the GRP to 0 under different load levels. Therefore, it is necessary to permit a tolerance band for gateway reactive power. Huang *et al.* [33] suggested to dynamically adjust the GRP according to load level at gateways between the 500 and 220 kV networks. However, this method does not apply to the situation under concern, as distributed wind power integration in the high-voltage distribution network makes the power loss characteristic more complex. In this case, the control effect of AVC depends highly on the rational setting of the control band for GRP, considering the influences of load level and wind power output variations.

The existing setting strategy for the control band of GRP [34] is based on empirical experience and can only realise rough balance rather than optimal distribution of reactive power in the entire network. The slack optimal control is therefore presented to set the slack control band of GRP according to the loss characteristic of single-source and double-source branch, thus to drive the power system's operation status close to optimal one, without changing the existing control frame.

3 Setting strategy for slack optimal control band of GRP

Considering that the fluctuation of wind power affects the voltage and power flow of the double-source branches, but not the single-source branches [3], the loss characteristics of these two types of branches are different.

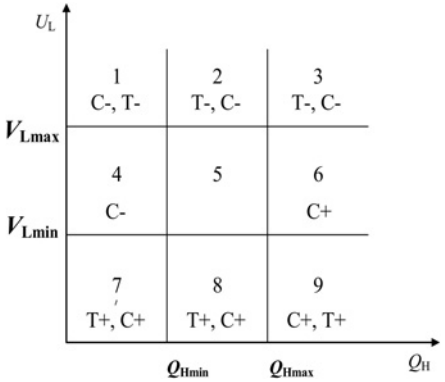

Fig. 2 *Nine-area control algorithm*

3.1 Loss characteristics of single-source branch

The total active power loss of a single-source branch, P_{LOSS}, can be expressed as

$$P_{LOSS} = \Delta P_T + \Delta P_L \tag{5}$$

where ΔP_T and ΔP_L are the active power loss of the transformer and the line in single-source branch, respectively, which are calculated from

$$\begin{aligned}\Delta P_T &= P_0 + P_k \frac{P_D^2 + (Q_H - \Delta Q_T)^2}{S_N^2} \\ &= P_0 + P_k\left[\beta^2 + \frac{(Q_H - \Delta Q_T)^2}{S_N^2}\right]\end{aligned} \tag{6}$$

$$\Delta Q_T = \frac{I_0\%}{100} S_N + \frac{V_k\%}{100}\frac{P_D^2 + (Q_H - \Delta Q_T)^2}{S_N} \tag{7}$$

where S_N is the transformer capacity; P_0 and P_k represent the zero-load and short-circuit loss of the transformer, respectively; $I_0\%$ and $V_k\%$ represent the percentages of zero-load current and short-circuit voltage, respectively; P_D and Q_D are active and reactive load demands, respectively; Q_C is the reactive power compensation of low-voltage side; ΔQ_T is the reactive power loss of the transformer; Q_H is the GRP; β is the active load rate of the transformer. The relationship between Q_H and Q_C can be

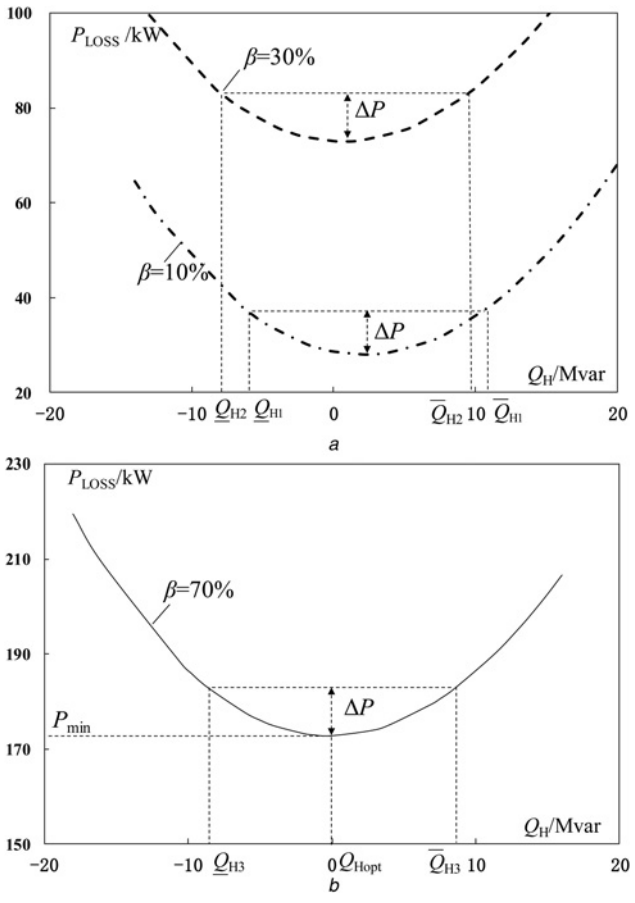

Fig. 3 *Characteristics of loss in the single-source branch*

a β = 10% and β = 30% in the single-source branch
b β = 70% in the single-source branch

IET Gener. Transm. Distrib., 2017, Vol. 11, Iss. 3, pp. 596–604

expressed by

$$Q_{\mathrm{H}} = Q_{\mathrm{D}} + \Delta Q_{\mathrm{T}} - Q_{\mathrm{C}} \tag{8}$$

The active power loss and reactive power loss of the line are given as

$$\Delta P_{\mathrm{L}} = \frac{(P_{\mathrm{D}} + \Delta P_{\mathrm{T}})^2 + (Q_{\mathrm{H}} - b_{\mathrm{L}} L V_{\mathrm{H}}^2/2)^2}{V_{\mathrm{H}}^2} r_{\mathrm{L}} l \tag{9}$$

$$\Delta Q_{\mathrm{L}} = \frac{(P_{\mathrm{D}} + \Delta P_{\mathrm{T}})^2 + (Q_{\mathrm{H}} - b_{\mathrm{L}} L V_{\mathrm{H}}^2/2)^2}{V_{\mathrm{H}}^2} x_{\mathrm{L}} l \tag{10}$$

where r_{L}, x_{L} and b_{L} are the unit resistance, reactance and susceptance of the line, respectively; l is the length of the line; ΔQ_{L} is the reactive power loss of the line; V_{H} is the voltage of high-voltage side of main transformer

$$V_{\mathrm{H}} = V_A - \frac{(P_{\mathrm{D}} + \Delta P_{\mathrm{T}}) r_{\mathrm{L}} l + (Q_{\mathrm{H}} - b_{\mathrm{L}} L V_{\mathrm{H}}^2/2) x_{\mathrm{L}} l}{V_{\mathrm{H}}} \tag{11}$$

where V_A is the voltage of the pilot bus.

Refer to (5)–(11), the operational variables that influence the active power loss of single-source branch are β and Q_{H}, when the parameters of the transformer and the line are given.

Therefore, P_{LOSS} can be expressed as an implicit function of Q_{H} and β

$$f(P_{\mathrm{LOSS}}, Q_{\mathrm{H}}, \beta) = 0 \tag{12}$$

where Q_{H} is the control variable which can be controlled by switching VAr compensation devices while β is the disturbance variable which depends on the load.

In a single-source branch, when β is determined, a U-shaped curve, which shows that P_{LOSS} varies with Q_{H}, can be obtained by adjusting reactive power compensation installed in the substation secondary bus. Such curves are shown in Figs. 3*a* and *b* when β is 10, 30 and 70%, respectively, for a specific single-source branch. The different curves correspond to the scenarios which represent different load levels, and the lowest points of the curves are essentially the extreme points of RPO to minimise the power loss, shifting from the right to the left of the abscissa as β increases. This means the heavier the active load demand, the less the reactive power consumption in the substation to reduce the active power loss of the single-source branch.

In Fig. 3*b*, P_{min} is the minimum active power loss of the branch under the specified scenario; Q_{Hopt}, corresponding to P_{min}, is defined as the optimal value of GRP; ΔP represents the maximum probable difference between the real P_{LOSS} and P_{min} when the GRP is controlled within the slack optimal band of GRP; $\bar{Q}_{\mathrm{H1}}$, $\bar{Q}_{\mathrm{H2}}$ and $\bar{Q}_{\mathrm{H3}}$ are the upper limits of slack optimal band of GRP when β are 10, 30 and 70%, respectively, while $\underline{Q}_{\mathrm{H1}}$, $\underline{Q}_{\mathrm{H2}}$ and $\underline{Q}_{\mathrm{H3}}$ represent the lower limits.

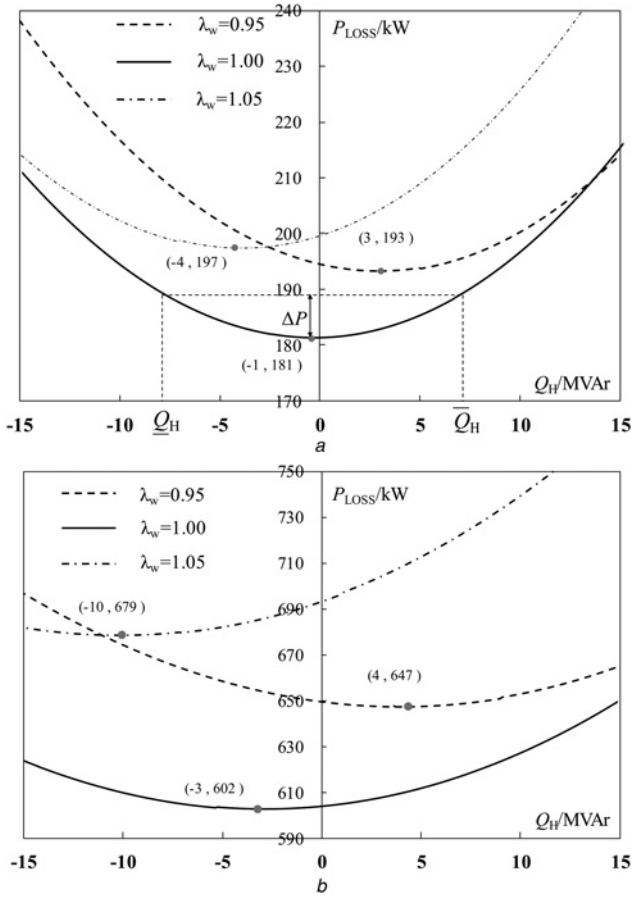

Fig. 4 *Characteristics of loss in the double-source branch*
a $P_{\mathrm{w}} = 0.5P_{\mathrm{w.max}}$ in the double-source branch
b $P_{\mathrm{w}} = P_{\mathrm{w.max}}$ in the double-source branch

3.2 Loss characteristics of double-source branch

Given that the active and reactive power outputs of the terminal wind farm will change the power flow of double-source branch, the characteristic of active power loss of the double-source branch is expressed as follows

$$g(P_{\mathrm{LOSS}}, Q_{\mathrm{H}}, \beta, P_{\mathrm{w}}, \lambda_{\mathrm{w}}) = 0 \tag{13}$$

where λ_{w} is the revised power factor of the wind farm, and its definition is given as follows

$$\lambda_{\mathrm{w}} = \begin{cases} \dfrac{P_{\mathrm{w}}}{\sqrt{P_{\mathrm{w}}^2 + Q_{\mathrm{w}}^2}} & Q_{\mathrm{w}} > 0 \\ -\dfrac{P_{\mathrm{w}}}{\sqrt{P_{\mathrm{w}}^2 + Q_{\mathrm{w}}^2}} + 2 & Q_{\mathrm{w}} < 0 \end{cases} \tag{14}$$

where P_{w} and Q_{w} are the active and reactive power outputs of the wind farm, respectively. Actually, λ_{w} is a conversion of power factor in order to differentiate the leading and the lagging power factors efficiently.

According to (13), the active power loss of the double-source branch will be influenced by the wind power outputs, load level and GRP. Among the above factors, the load level and the wind power outputs are uncontrollable variables with certain randomness, so the active loss of the distribution system is mainly decided by Q_{H}, which is controlled by switching reactive power compensators installed in secondary bus of substation.

Similarly, the U-shaped curves of P_{LOSS} varying with Q_{H} for a specific double-source branch with different P_{w} and λ_{w} are shown in Figs. 4*a* and *b*, where $P_{\mathrm{w.max}}$ represents the maximum active power output of the wind farm. It is obvious from the curves that Q_{Hopt} changes when the output of the wind farm changes.

As shown in Figs. 3 and 4, the curves are gentle in the bottom relatively, while become steep on both sides. Consequently, the system loss is low enough when the GRP is controlled in the neighbourhood of the lowest point of U-shaped curves which are marked by grey dots in Figs. 4*a* and 4*b*. On the other hand, the wider tolerance control band of GRP will result in less adjustment of reactive power compensation devices. Considering the objective of saving energy, improving voltage profile and decreasing frequency of control devices regulation, it is necessary to set a reasonable allowable control band of GRP in single-source and double-source branches.

3.3 Slack optimal control band of GRP in single-source branch

As shown in Fig. 3*b*, the value of Q_{Hopt} changes with β in the single-source branch. To ensure the system runs near the optimal point under various load levels, the slack optimal active loss difference (ΔP) strategy is proposed in this paper to set the slack optimal bands of GRP of substation in the single-source branch.

The slack optimal active loss difference, ΔP, is expressed as

$$\Delta P = \alpha P_{\min 3} \tag{15}$$

where $P_{\min 3}$ is the minimum power loss of the single-source branch in theory when $\beta = 70\%$. For safe and reliable operation, β is usually less than 70% in any substation. The width of the GRP band is decided by ΔP distinctly.

According to the simulation studies, β has a small influence to the boundary of slack optimal bands of GRP in single-source branches. In order to make the control method simple and reliable, the slack optimal bands of GRP are only classified according to two typical conditions: light and not-light loads. The setting procedure of slack optimal bands of GRP is described as follows:

Step 1: Collect the parameters of lines and transformers.
Step 2: The relationship of P_{LOSS} and Q_{H} are drawn up according to Figs. 3*a* and *b* for different typical conditions, such as $\beta = 10\%$, $\beta = 30\%$ and $\beta = 70\%$, which represent three typical load levels. The constant ΔP, which is decided by (15), is obtained based on $P_{\min 3}$.
Step 3: Calculate the initial slack optimal bands of GRP under three typical conditions based on the $P_{\min}$ and ΔP.
Step 4: If $\underline{Q}_{\text{H1}} < 0$, let $\underline{Q}_{\text{H1}} = 0$ to avoid the reverse reactive power flow when $\beta = 10\%$.
Step 5: The intersection of slack optimal bands of GRP of $\beta = 10\%$ and $\beta = 30\%$ is set as the slack optimal band of GRP under light load conditions (i.e. $\beta <= 30\%$), while the intersection of slack optimal bands of GRP of $\beta = 30\%$ and $\beta = 70\%$ is set as the slack optimal band of GRP under not-light load conditions (i.e. $\beta \geq 30\%$).

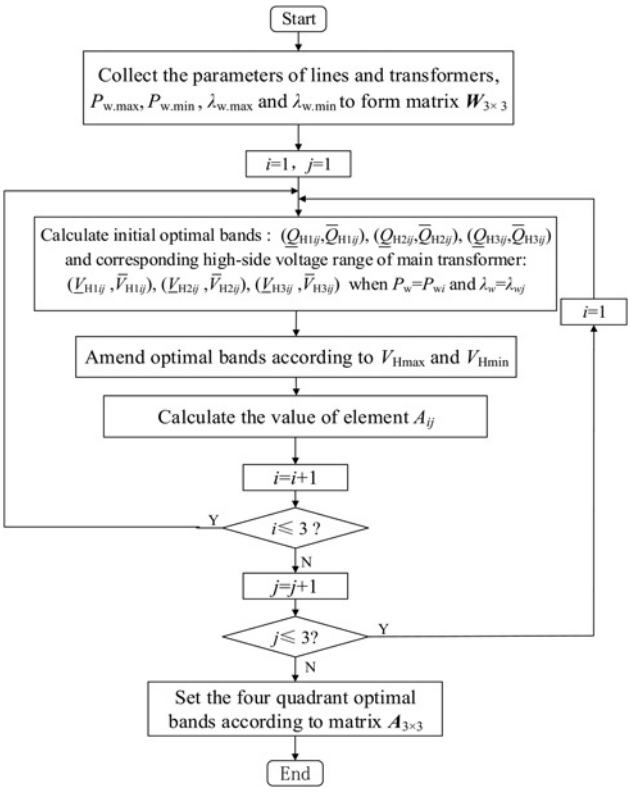

Fig. 5 *Flowchart of slack optimal band setting of GRP in a double-source branch*

3.4 Slack optimal control band of GRP in double-source branch

The Q_{Hopt} in a double-source branch changes with β, P_{w} and λ_{w}, among which P_{w} and λ_{w} are main influence factors. The flowchart of the slack optimal band of GRP setting strategy for double-source branches is shown in Fig. 5.

In Fig. 5, $\boldsymbol{W}_{3\times3}$ is defined as the wind farm operating condition matrix, which is composed of different scenarios in which the active and reactive power outputs of the wind farm changes from small to large. The specific formula is described as follows

$$\begin{aligned}\boldsymbol{W}_{3\times3} &= \begin{bmatrix} W_{11} & W_{12} & W_{13} \\ W_{21} & W_{22} & W_{23} \\ W_{31} & W_{32} & W_{33} \end{bmatrix} \\ &= \begin{bmatrix} (P_{w1}, \lambda_{w1}) & (P_{w1}, \lambda_{w2}) & (P_{w1}, \lambda_{w3}) \\ (P_{w2}, \lambda_{w1}) & (P_{w2}, \lambda_{w2}) & (P_{w2}, \lambda_{w3}) \\ (P_{w3}, \lambda_{w1}) & (P_{w3}, \lambda_{w2}) & (P_{w3}, \lambda_{w3}) \end{bmatrix}\end{aligned} \tag{16}$$

The element W_{ij} of $\boldsymbol{W}_{3\times3}$ represents the specific operating condition of the wind farm when $P_{\text{w}} = P_{\text{w}i}$ and $\lambda_{\text{w}} = \lambda_{\text{w}j}$, where $P_{\text{w1}} = P_{\text{w.max}}$, $P_{\text{w3}} = P_{\text{w.min}}$, $P_{\text{w2}} = (P_{\text{w.max}} + P_{\text{w.min}})/2$, $\lambda_{\text{w1}} = \lambda_{\text{w.min}}$, $\lambda_{\text{w3}} = \lambda_{\text{w.max}}$ and $\lambda_{\text{w2}} = (\lambda_{\text{w.max}} + \lambda_{\text{w.min}})/2$. The subscripts max and min mean the maximum and minimum values, respectively.

In Fig. 5, $\boldsymbol{A}_{3\times3}$, which is composed of a series of slack optimal bands of GRP, is defined as slack optimal band matrix. The physical meaning of element A_{ij} in $\boldsymbol{A}_{3\times3}$ is the intersection of the voltage-amended slack optimal bands of GRP under three conditions when $P_{\text{w}} = P_{\text{w}i}$ and $\lambda_{\text{w}} = \lambda_{\text{w}j}$, as formulated by

$$A_{ij} = (\underline{Q}'_{\text{H1}ij}, \overline{Q}'_{\text{H1}ij}) \cap (\underline{Q}'_{\text{H2}ij}, \overline{Q}'_{\text{H3}ij}) \cap (\underline{Q}'_{\text{H2}ij}, \overline{Q}'_{\text{H3}ij}) \tag{17}$$

where the subscript numbers 1, 2 and 3 correspond to β being 10, 30 and 70%, respectively, and the superscription ($'$) means the amended upper or lower limit of slack optimal band of GRP in consideration of substation primary bus voltage security based on the boundary value derived from the slack optimal active loss difference (ΔP) strategy.

It is highlighted here that the upper and lower limits of the optimal band of GRP should be amended to ensure the substation primary bus voltage (i.e. V_{H}) within a secure range ($V^{\min} + \varepsilon$, $V^{\max} - \varepsilon$), since wind power integration tends to cause over-limit voltage in the double-source branch. The procedure will be illustrated in the following section.

Each element in $\boldsymbol{A}_{3\times3}$ only represents the specific slack optimal band of GRP under a typical scenario. To ensure the setting of slack optimal band parameters of GRP can cover most operating conditions, partitioning intersection algorithm is proposed in this paper. In this algorithm, $\boldsymbol{A}_{3\times3}$ is partitioned by two dimensions including P_{w} and λ_{w}, and the cut-off point is (P_{w2}, λ_{w2}), and the four typical slack optimal bands of GRP can be set by taking the

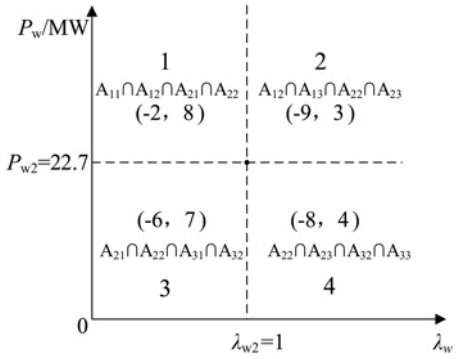

Fig. 6 *Partitioning intersection algorithm*

IET Gener. Transm. Distrib., 2017, Vol. 11, Iss. 3, pp. 596–604

Table 1 Parameters of lines

Line	Length, km	Resistance, Ω	Reactance, Ω	Susceptance, S
L_1	15	1.2	6.26	41.1
L_2	10	0.8	4.17	27.4
L_3	20	2.64	7.72	59.2

intersection of the corresponding elements of matrix $\boldsymbol{A}_{3\times3}$ as shown in Fig. 6.

4 Case studies

4.1 Setting of slack optimal band of GRP for typical situation

To illustrate the proposed setting strategy, a 110 kV single-source branch and a 110 kV double-source branch are used in this section, and the whole system is configured as shown in Fig. 1. The voltage of pilot bus, E_S, is 115 kV, X'_S is the equivalent reactance and the models of transformer T_D and T_C are both SFZ9-50000/110, whose parameters are listed as follows: P_k = 194.4 kW, P_0 = 36.3 kW, $U_k\%$ = 10.5 and $I_0\%$ = 0.35. The parameters of the lines are shown in Table 1.

The installed capacity of wind power farm F is 49.5 MW and P_w varies from 4.95 to 49.5 MW randomly. Considering the power factors of wind farms are restricted within the range of 0.95 leading to 0.95 lagging [35, 36] and are usually controlled by the distributed wind farms rather than by the distribution system operator, λ_w varies from 0.95 to 1.05 randomly. Here, λ_w = 1.05 means the power factor is 0.95 leading, while λ_w = 0.95 means the power factor is 0.95 lagging.

4.1.1 Single-source branch: The optimal bands of GRP at Substation D in the single-source branch are calculated according to the setting strategy mentioned in Section 3.3. At the first stage, Q_{Hopt} and P_{min} under different load levels are solved and the results are listed in Table 2.

Let α = 4%; therefore, $\Delta P = \alpha P_{min3}$ = 0.04*234 kW ≃9 kW. The initial slack optimal bands of GRP are obtained based on the loss curves and the value of ΔP, as depicted in Fig. 3*b*. Then, the slack optimal bands of GRP are rounded and amended to avoid reverse reactive power under light load conditions according to Step 4 described in Section 3.3. The results are shown in Table 3.

For the convenience of engineering application, two control parameters for slack optimal control under light and not-light loads conditions can be set according to the intersections of the slack optimal control bands in Table 3, as shown in Table 4.

4.1.2 Double-source branch: The slack optimal bands of GRP at Substation C in the double-source branch are set according to Fig. 5. The key issue is to calculate $\boldsymbol{A}_{3\times3}$. Given ε = 0.1 p.u. and α = 4%, this section takes element A_{11} as an example to explain the specific calculation process.

The value of A_{11} is calculated from W_{11}, and $W_{11} = (P_{w1}, \lambda_{w1})$ = (49.5, 0.95). In this status, both the active and reactive power outputs of the wind farm reach the maximum.

When β = 70%, the relationships of P_{LOSS}, V_{HC} (the primary bus voltage of Substation C) and Q_{HC} (the GRP of Substation C) are derived by load flow computation, and the curves are shown in Fig. 7, where Q_{Hopt} = 3.8 MVAr and P_{min3} = 673 kW. Hence, $\Delta P = \alpha P_{min3}$ = 0.04*673 ≃27 kW. The initial optimal band of GRP is (−10.1, 17.4) and the corresponding band of V_{HC} is (114.9, 117.0) consequently. Considering the voltage constraint $V_{HC} \le 116.6$ kV, the slack optimal band of GRP is modified to (−4.8, 17.4). In the same way, the initial and amended optimal bands of GRP under varied road levels can be obtained and the results are shown in Table 5.

Therefore, $A_{11} = (-5, 17) \cap (-4, 17) \cap (-2, 17) = (-2, 17)$. In the same way, other elements in $\boldsymbol{A}_{3\times3}$ are obtained

$$\boldsymbol{A}_{3\times3} = \begin{bmatrix} A_{11} & A_{12} & A_{13} \\ A_{21} & A_{22} & A_{23} \\ A_{31} & A_{32} & A_{33} \end{bmatrix} = \begin{bmatrix} (-2, 17) & (-16, 10) & (-24, 3) \\ (-6, 11) & (-9, 8) & (-13, 4) \\ (-7, 7) & (-8, 7) & (-8, 6) \end{bmatrix}$$

The four typical slack optimal bands of GRP are therefore obtained and shown in Table 6 according to the partitioning intersection algorithm as depicted in Fig. 6.

4.2 Practical case

A real 110 kV distribution network in Guangdong province, China is studied in this section. The network contains a wind farm and its structure is shown in Fig. 1. The pilot bus A is the 110 kV bus of a 220 kV substations, B, C, D and E are four 110 kV substations, F is a distributed wind farm rated 49.5 MW, X_S is the equivalent reactance of the upper power system, and E_S is the equivalent voltage potential. Q_S is the reactive power injected to the 110 kV distribution network from 220 kV transmission power grid. Switched capacitor banks are installed at each 10 kV bus. Each capacitor bank has a rating of ten MVAr and two stages of five MVAr each. The total loads and the outputs of the wind farm in a certain day are shown in Fig. 8.

The upper and lower limits of V_L of the nine-area control algorithm are set to 10.6 and 10.1 kV, respectively. Three methods are applied to set the upper and lower limits of Q_H and the results are given in Table 7. The three methods are described as follows:

(i) *Method 1:* The setting values of each substation are derived from the standard [34]. According to the standard, the power factor of substation primary bus should be higher than 0.95 lagging under not-light load conditions, while it should be lower than 0.95 lagging under light load conditions. This is the most common setting strategy for GRP control bands of 110 kV substations used in China currently.
(ii) *Method 2:* The control bands for GRP of each substation are given according to Table 4 without differentiating between the different kinds of branches. It is based on the loss characteristics of the given network under different load levels, while method 1 is based on the empirical rule.
(iii) *Method 3:* The setting values of the substations in single-source branches are given according to Table 4, while those in double-source branches are given according to Table 6. This

Table 2 Q_{Hopt} and P_{min} under different load levels

β, %	Q_{Hopt}, MVAr	P_{min}, kW
10	0.21	29
30	0.02	93
70	−0.38	234

Table 3 Slack optimal bands of GRP under different load levels

β, %	Initial	Amended
10	(−6.8, 8.2)	(0, 8)
30	(−7.2, 7.7)	(−7, 8)
70	(−7.6, 7.2)	(−8, 7)

Table 4 Slack optimal bands of GRP for Substation D

Load	Slack optimal band, MVAr
light load (β < 30%)	(0, 8)
not light load ($\beta \ge$ 30%)	(−7, 7)

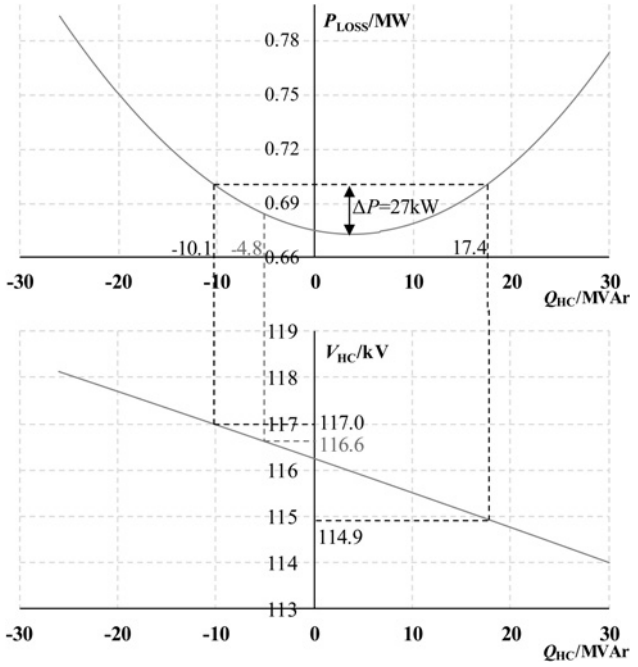

Fig. 7 *Curves of P_{LOSS} and V_{HC} when $\beta = 70\%$*

method considers the loss characteristics of the given network under different load levels and wind farm outputs.

Based on the nine-area algorithm and the different GRP control bands mentioned in Table 7, simulation studies of 96 states in a day (with a 15-min time interval between two subsequent states) are carried out using C# programming. The simulation results are shown in Table 8. These results are compared with the RPO aiming at minimisation of active power loss [30], and the IVVC method and the control parameters of IVVC are pre-set at $Q_{Limit} = 10$ and $Q_{Status} = 2$ [25]. Furthermore, simulation results are demonstrated in Fig. 9, including the curves of the voltage of the bus of wind farm integration (V_W), GRP of Substation C (Q_{HC}), GRP of Substation B (Q_{HB}) and Q_S curves using different local control methods.

In Table 8, W is the daily energy loss of the network, measured in kWh; N_T and N_C are the daily regulation times of all on-load tap changers and all of switch capacitor banks in the network, respectively; N_{total} represents the sum of N_T and N_C; V% is the voltage qualified rate of V_w all day; C_A represents the cost of adjusting the discrete control devices, measured in kW, and the unit adjustment cost of OLTC tap and compensator are set to 10 and 6 kW/times, respectively, according to [30]. It's important to note that the unit adjustment cost of OLTC tap is more than that of reactive compensator.

So far, some conclusions can be drawn from the simulation studies as follows:

Table 5 Slack optimal control bands of GRP under different loads

β, %	Initial	Amended	Rounded
70	(−10.1, 17.4)	(−4.8, 17.4)	(−5, 17)
30	(−10.0, 17.3)	(−3.7, 17.3)	(−4, 17)
10	(−9.8, 17.2)	(−2.4, 17.2)	(−2, 17)

Table 6 Slack optimal bands of GRP for Substation C

Optimal band, MVAr, MW	$\lambda_w < 1$	$\lambda_w \geq 1$
$Pw \geq 22.7$	(−2, 8)	(−9, 3)
$Pw < 22.7$	(−6, 7)	(−8, 4)

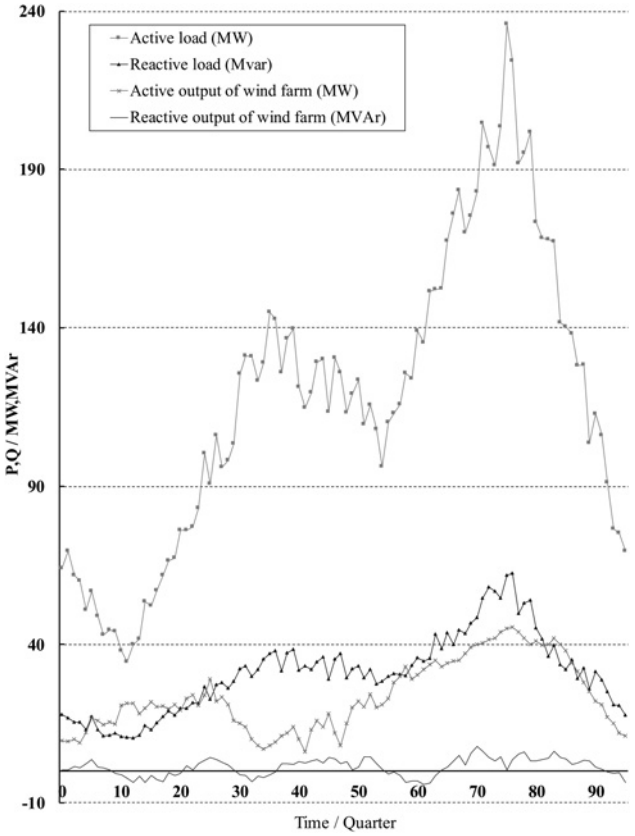

Fig. 8 *Load and output power curves*

(i) *Energy saving:* The daily energy loss obtained by the conventional control method (Method 1) is the highest while that by RPO is the lowest, and the loss control by the proposed method (Method 3) is less than those by other local control methods. Thus it can be seen that the loss can be lowered when the GRP control band is set according to the loss-load characteristics and the loss-wind power characteristics. Compared with the loss by Method 1 and IVVC, the loss by Method 3 is reduced by 2.3–3.2%, which is only 2.1% higher than the loss by RPO, a typical centralised control method.

(ii) *Regulation times of discrete control devices:* The total times by method 3 are the second lowest, but the cost of adjusting the control devices by the proposed method is the least due to less OLTC

Table 7 GRP control bands of three methods

Substation	β	Method 1	Method 2	Method 3
D, E	light load ($\beta < 30\%$)	(2, 11)	(0, 8)	(0, 8)
	not-light load ($\beta \geq 30\%$)	(−11, 11)	(−7, 7)	(−7, 7)
B, C	light load ($\beta < 30\%$)	(2, 11)	(0, 8)	refer to Table 6
	not-light load ($\beta \geq 30\%$)	(−11, 11)	(−7, 7)	

Table 8 Control effect of different methods

Method	W, kWh	N_T	N_C	N_{total}	V, %	C_A, kW
method 1	21,573	22	14	36	100	304
method 2	21,013	15	26	41	96.9	306
method 3	20,882	10	25	35	100	250
IVVC	21,355	25	7	32	100	292
RPO	20,450	325	101	426	100	3856

IET Gener. Transm. Distrib., 2017, Vol. 11, Iss. 3, pp. 596–604

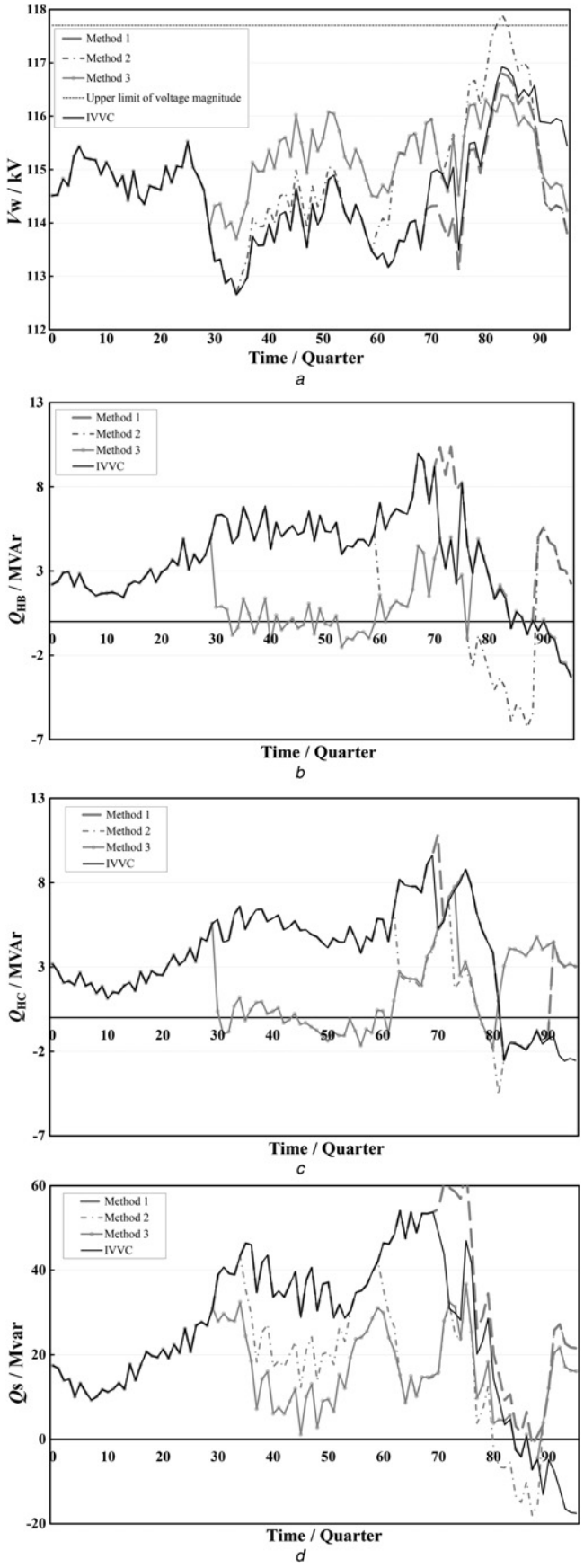

Fig. 9 *V_w, Q_{HB}, Q_{HC} and Q_S, using different methods*

a V_w the voltage of the bus of wind farm integration
b Q_{HB} GRP of Substation B
c Q_{HC} GRP of Substation C
d Q_S the reactive power injected to the 110 kV distribution network from 220 kV power grid

adjusting than by IVVC. The total times by RPO are over ten times higher than other methods, which is unbearable for distribution system operators and it may threaten the security of system seriously. Hence RPO is not applicable for the voltage and reactive control in distribution networks with wind farm integration.

(iii) *Voltage quality:* It can be seen from Fig. 9*a* that V_w calculated by Method 3 is among [113.7, 116.4] kV all day long and has more margins than that by other methods. The reason for this result is that different control method for GRP of Substations C and B causes the difference of Q_{HC} and Q_{HB} at some time which is related to the voltage profile in high-voltage distribution networks. As shown in Figs. 9*b* and *c*, from 0 a.m. to 7:30 a.m., four methods have similar control effect for GRP in Substations C and B under light load and low wind farm output conditions. From 7:30 a.m. to 3 p.m., the reactive power consumption in Substations C and B is only reduced by Method 3, to maintain the voltage level and reduce the network loss under middle load and low wind farm output conditions. From 3 p.m. to 8 p.m., the reactive power consumption slightly increases in Substations C and B, under the control of Method 3, to decrease the voltage fluctuation when the wind farm output gradually increases during this time. From 8 p.m. to 12 p.m., with the loads decrease and wind farm outputs increase, voltage violation occurs if Method 2 is applied; however, the violation can be avoided by Method 3.

(iv) *Reactive power balance:* The variation range of Q_S obtained by Method 3, as shown in Fig. 9*d*, is [−6.9, 36.7] MVAr. It is smaller than that obtained by other methods, which will be more beneficial to the reactive power local balance.

To sum up, it is Method 3 that realises the multi-objective volt/VAr control including saving energy, improving voltage quality and reducing adjustment cost, for this method considers the loss characteristics of the given network under different load conditions and various wind power outputs.

5 Conclusions

This paper proposes an efficient and practical method for voltage and reactive power regulation by using substation shunt capacitors and OLTC in high-voltage distribution networks with distributed wind farms integration. Both the load levels and wind power outputs are considered in the proposed method. Based on numerical analysis, we can conclude that the GRP slack optimal control bands of substations in the single-source branch should be set according to different load levels and the setting strategy for GRP slack optimal control bands of substations in the double-source branch should consider the changing of wind power outputs additionally. With the load level of distribution system and the output range of the wind power farm considered, the differential slack optimal control bands of GRP are worked out based on the slack optimal control method. The simulation results show that the energy loss of the proposed method can be reduced by 2.3–3.2% in comparison with the existing method. Moreover, fewer regulation times and better voltage profile can be obtained by the proposed method, indicating that the proposed method is efficient for distribution operations and helps to improve power quality.

6 Acknowledgments

The authors give their sincere appreciations to the support of National Natural Science Foundation of China (no. 51377060).

7 References

1 'World Wind Energy Association'. http://www.wwindea.org/world-wind-energy-report-2011-launched, 2011
2 Gao, H.X., Chen, L.J., Chen, Y., *et al.*: 'A scenario-based evaluation framework and its implementation for wind farm integration in distribution work'. Proc. IEEE Int. Conf. Power System Technology, Auckland, New Zealand, October 2012, pp. 1–6

3 Liu, L., Zhang, Y.J., Zhu, H.J.: 'Conductor selection of transmission line connected to wind farm considering the operation characteristic'. Proc. IEEE Int. Conf. Power and Energy Engineering, Kowloon, December 2013, pp. 7–15
4 Ammar, M., Joos, G.: 'A short-term energy storage system for voltage quality improvement in distributed wind power', *IEEE Trans. Energy Convers.*, 2014, **29**, (4), pp. 997–1007
5 Ammar, M., Joos, G.: 'Impact of distributed wind generators reactive power behavior on flicker severity', *IEEE Trans. Energy Convers.*, 2013, **28**, (2), pp. 425–433
6 Jason, M.S., Salman, M.: 'Voltage quality assessment in a distribution system with distributed generation-a probabilistic load flow approach', *IEEE Trans. Power Deliv.*, 2013, **28**, (3), pp. 1652–1662
7 Victor, H.Q., Juan, R.A., Tomas, G.S.R.: 'Assessment of energy distribution loss for increasing penetration of distributed generation', *IEEE Trans. Power Syst.*, 2006, **21**, (2), pp. 533–540
8 Haque, M.H.: 'Voltage profile and loss assessment of distribution systems with fixed speed wind generators'. Proc. IEEE Int. Conf. Innovative Smart Grid Technologies, Kuala Lumpur, May 2014, pp. 210–215
9 Salih, S.N., Chen, P.Y., Carlson, O.: 'The effect of wind power integration on the frequency of tap changes of a substation transformer', *IEEE Trans. Power Syst.*, 2013, **28**, (4), pp. 4320–4327
10 Baghsorkhi, S., Hiskens, I.: 'Impact of wind power variability on sub-transmission networks'. Master's thesis, Lund Univ., Lund, Sweden, 2016
11 Kulmala, A., Repo, S., Jarventausta, P.: 'Coordinated voltage control in distribution networks including several distributed energy resources', *IEEE Trans. Smart Grid*, 2014, **5**, (4), pp. 2010–2020
12 Shaheen, A.M., EI-Sehiemy, R.A., Farrag, S.M.: 'A novel adequate bi-level reactive power planning strategy', *Int. J. Electr. Power Energy Syst.*, 2015, **78**, pp. 897–909
13 Ouammi, A., Dagdougui, H., Sacile, R.: 'Optimal control of power flows and energy local storages in a network of microgrids modelled as a system of systems', *IEEE Trans. Control Syst. Technol.*, 2015, **23**, (1), pp. 128–138
14 Ding, T., Liu, S.L., Yuan, W., *et al*.: 'Two-stage robust reactive power optimization considering uncertain wind power integration in active distribution networks', *IEEE Trans. Power Syst.*, 2016, **7**, (1), pp. 301–311
15 Zhao, J.J., Li, Z.K., Li, D.D.: 'Reactive power optimization algorithm of considering wind farm voltage control capability in distribution system'. Proc. IEEE Int. Conf. Electrical Machines and Systems, Beijing, China, August 2011, pp. 1–4
16 Jiang, Z.H., Li, N.H., Yao, M.Q.: 'Dynamic optimization of reactive power and voltage control in distribution network considering the connection of DFIG'. Proc. IEEE Int. Conf. Power Engineering and Automation, Wuhan, China, September 2011, pp. 30–34
17 Chen, R.Z., Sun, H.B., Guo, Q.L., *et al*.: 'Reducing generation uncertainty by integration CSP with wind power: an adaptive robust optimization-based analysis', *IEEE Trans. Sustain. Energy*, 2015, **6**, (2), pp. 583–593
18 Yorino, N., Zoka, Y., Watanabe, M., *et al*.: 'An optimal autonomous decentralized control method for voltage control devices by using a multi-agent system', *IEEE Trans. Power Syst.*, 2015, **30**, (5), pp. 2225–2233
19 Ahmed, H.: 'Reactive power and voltage control in grid-connected wind farms: an online optimization based fast model predictive control approach', *Electr. Eng.*, 2015, **97**, (1), pp. 35–44
20 Elmitwally, A., Elsaid, M., Elgamal, M., *et al*.: 'A fuzzy-multiagent self-healing scheme for a distribution system with distributed generations', *IEEE Trans. Power Syst.*, 2015, **30**, (5), pp. 2612–2622
21 Salih, S.N., Chen, P.Y.: 'On coordinated control of OLTC and reactive power compensation for voltage regulation in distribution systems with wind power', *IEEE Trans. Power Syst.*, 2015, **31**, pp. 1–10
22 Choi, J.H., Moon, S.I.: 'Design of the optimal ULTC parameters in distribution system with distributed generations', *IEEE Trans. Power Syst.*, 2009, **24**, (1), pp. 319–326
23 Kim, M., Hara, R., Kita, H.: 'Design of the optimal ULTC parameters in distribution system with distributed generations', *IEEE Trans. Power Syst.*, 2009, **24**, (1), pp. 297–305
24 Muttaqi, K.M., Negnevitsky, M., Ledwich, G.: 'A coordinated voltage control approach for coordination of OLTC, voltage regulator, and DG to regulate voltage in a distribution feeder', *IEEE Trans. Ind. Appl.*, 2015, **51**, (2), pp. 1239–1248
25 Afandi, I., Ciufo, P., Agalgaonkar, A., *et al*.: 'A comparison of voltage regulation and control methods'. Proc. IEEE Int. Conf. Power Engineering, Wollongong, September 2015, pp. 1–6
26 Viawan, F.A., Karlsson, D.: 'Voltage and reactive power control in systems with synchronous machine-based distributed generation', *IEEE Trans. Power Deliv.*, 2008, **23**, (2), pp. 1079–1087
27 Mei, S.W., Xie, B.P., Che, W.Y., *et al*.: 'Hybrid automatic voltage control strategy and its application to northeast china 500 kV power grid', *Eur. Trans. Electr. Power*, 2009, **19**, (3), pp. 355–367
28 Li, J.H., Zou, J.X.: 'Research on the coordination control between STATCOM and VQC in substation based on the identification of system state', *Adv. Mater. Res.*, 2014, **905**, pp. 1239–1248
29 Askarzadeh, A.: 'Capacitor placement in distribution systems for power loss reduction and voltage improvement: a new methodology', *IET Gener. Transm. Distrib.*, 2016, **10**, pp. 1–8
30 Zhang, Y.J., Ren, Z.: 'Optimal reactive power dispatch considering costs of adjusting the control devices', *IEEE Trans. Power Syst.*, 2005, **20**, (3), pp. 1349–1356
31 Xu, Z.G., Wang, F.: 'Research on fuzzy logic based dynamic boundary voltage and reactive power integrated control method'. Proc. IEEE Int. Conf. Control and Decision, Guilin, China, June 2009, pp. 1645–1649
32 Zhang, Y.J., Li, Q.H., Chen, X.: 'Reactive power optimization oriented control using optimal reactive power supply for radial network'. Proc. IEEE Int. Conf. Region 10 Symp., Kuala Lumpur, April 2014, pp. 492–495
33 Huang, M., Zhang, Y.J., Zhang, X.T., *et al*.: 'Reactive power coordinated control at the gateway between provincial and regional power grids'. Proc. IEEE Int. Conf. Power and Energy Engineering, Kowloon, December 2013, pp. 1–6
34 Energy Department standard of the People's Republic of China SD 325-1989: 'Guidelines on power system voltage and reactive power techniques'. [in Chinese]
35 Sansawatt, T., Ochoa, L.F., Harrison, G.P.: 'Smart decentralized control of DG for voltage and thermal constraint management', *IEEE Trans. Power Syst.*, 2012, **27**, (3), pp. 1637–1645
36 No. RM05-4-000: 'Interconnection for Wind Energy and Other Alternative Technologies'. Docket, 2005